Passive Quadrupedal Bounding with a Segmented Flexible Torso*

Qu Cao and Ioannis Poulakakis

***Abstract*— This paper examines the effect of torso flexibility on the dynamics of quadrupedal running with a bounding gait. A reduced-order passive and conservative model with a segmented flexible torso and compliant legs is introduced to study torso-leg coordination. Numerical return map studies reveal that a large variety of cyclic bounding motions can be realized passively, as a natural mode of the system. Despite the simplicity of the model, the resulting motions correspond to torso bending movements that resemble those in galloping mammals without explicit reliance on the fine structural and morphological details. This way, the proposed model offers a unifying description of the task-level locomotion behavior, and can be used to inform feedback control synthesis by serving as a behavioral target for the control system.**

I. Introduction

Out of the many reasons for exploring the use of legged robots one stands out: mobility. A diverse set of ingenious and inspiring legged robots has been introduced over the past 40 years to investigate the prospect of such machines in a variety of real-world applications. In this class of robots, quadrupeds offer a good tradeoff among stability, load-carrying capacity, and mechanical complexity. These properties render machines of this kind an attractive alternative to conventional vehicles when enhanced mobility is needed.

Raibert and his collaborators were the first to report on actively-balancing legged robots including quadrupeds [1]. In the same vein, the Scout II quadruped demonstrated efficient running motions using only one actuator per leg [2]. More recently, BigDog exhibited impressive rough-terrain mobility using controllers that combine Raibert's approach with virtual model control ideas [3]. A different paradigm employing fuzzy logic control informed by Raibert-style heuristics has been introduced in [4] to investigate running on the quadrupedal robot KOLT introduced in [5].

In contrast to their counterparts in nature—which owe much of their remarkable locomotion performance to their flexible torsos and limbs—running robotic quadrupeds incorporate rigid, non-deformable torsos. Exceptions to this general rule are rare. Early work on introducing passive or articulated segmented torsos in legged platforms includes walking quadrupeds [6], [7] and hopping and hybrid wheeled-legged systems [8]. However, these efforts focus primarily on platform design and, in general, do not consider dynamic running motions and modeling issues.

*This work is supported in part by NSF grant CMMI-1130372 and ONR contract W911NF-12-1-0117.

A video of the results of Section III accompanies the paper.

Q. Cao and I. Poulakakis are with the Department of Mechanical Engineering, University of Delaware, Newark, DE 19716, USA; e-mail: {caoqu, poulakas}@udel.edu.

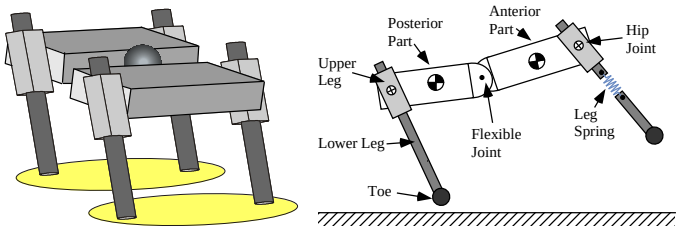

Fig. 1. (a) A three-dimensional virtual prototype of a quadrupedal robot with a segmented torso. (b) A sagittal-plane model for studying the effect of torso bending motions on the bounding running gait.

Despite consensus that torso flexibility can improve performance in a variety of dynamically-stable locomotion behaviors—see [8] and references therein—only limited information is available on reductive robot models that can capture such capabilities. The vast majority of modeling efforts focus primarily on models with rigid, non-deformable torsos. Examples include [9]–[12], which investigate conditions for generating and sustaining cyclic bounding motions on passive reduced-order models. More complete models capable of various running gaits also exist in the literature; see [13]–[15] for examples of such models. However, with the exception of [14], which incorporates elastic structures in the back and neck of a horse model, and [15] and [16], which consider an actuated spine, none of these models include torso bending motions.

Much of the work on how torso flexibility affects locomotion performance has been developed in the context of biomechanics. Early studies on the horse and the cheetah demonstrate the significance of the flexible torso in increasing traveling speed, and provide a phenomenological description of the coordination between the torso's sagittal movements and leg recirculation [17]. In addition to enhancing performance, elastic elements located in the torso may reduce the metabolic cost of transport through recycling part of the kinetic energy required to recirculate the legs [18]. Finally, recent studies in [19] put forward the hypothesis that sagittal plane spinal oscillations may improve gait stability through the effective implementation of self-stabilizing mechanisms that rely on adjusting the angle and angular rate of a leg prior to its touchdown.

Translating such intuitive biomechanical observations into reduced-order models that can inform feedback control synthesis for high-performance legged robots with flexible torsos constitutes the goal of this work. As a first step toward this goal, this paper introduces a conservative sagittal-

plane model of quadrupedal bounding, which incorporates a segmented flexible torso and compliant legs; see Fig. 1. Conditions that permit the passive generation of cyclic bounding running are identified through numerical studies of a Poincaré return map, and a large number of such motions is computed. It is shown that within the same total energy level, a range of average forward speeds can be realized depending on the touchdown angles of the anterior and posterior legs.

The structure of the paper is as follows. Section II introduces the model and derives a Poincaré return map whose fixed points correspond to the bounding running motions of interest. Section III discusses in detail the properties of a large number of cyclic bounding motions, and provides a discussion of the local stability properties of the computed gaits. Section IV concludes the paper.

II. Bounding with a Segmented Torso

To study the effect of a segmented torso on the dynamics of the bounding gait, the sagittal-plane model depicted in Figs. 1(b) and 2 is introduced. In this model, the torso consists of two identical rigid bodies; one represents its posterior (caudal) and the other its anterior (cranial) part. The two rigid bodies are connected through a rotational spring, intended to introduce flexibility in the segmented torso. Despite its simple lumped nature, the proposed model is capable of realizing torso sagittal bending movements that resemble spinal flexion and extension motions in galloping mammals; see [17], [20] for descriptions of such gaits. In this work we concentrate on how the targeted gait behavior can be generated naturally; that is, as an intrinsic property of the model. Therefore, input motor torques and energy dissipation forces acting in continuous time are not considered.

In modeling the dynamics of the model of Fig. 2, it is assumed that both parts of the torso have mass m and moment of inertia J about their center of mass (COM), and that are interconnected via a rotational spring with stiffness k_{torso}. The legs are assumed to be massless springs of stiffness k_{leg}, and their contact with the ground is modeled as an unactuated, frictionless pin joint. The mechanical properties of the model used in the simulations are presented in Table I, and they roughly correspond to the geometry of the quadrupedal robot Scout II; see [2], [9].

For brevity, in this paper we restrict our attention to the

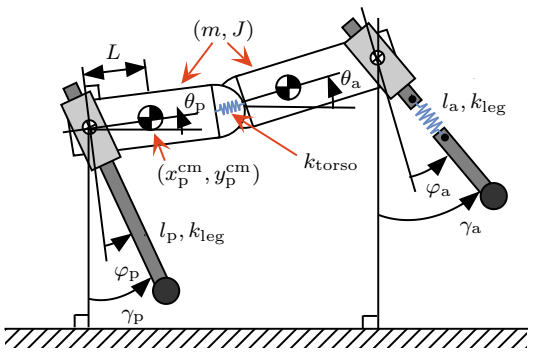

Fig. 2. A sagittal-plane bounding model with a segmented torso.

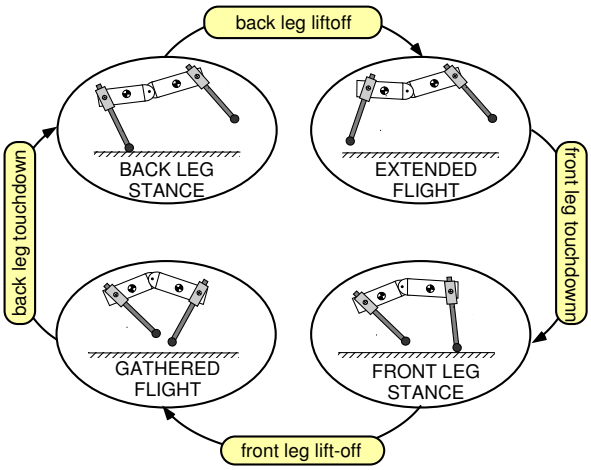

Fig. 3. Bounding phases and events.

bounding gait presented in Fig. 3. Depending on the state of a leg—stance or flight—we distinguish the following phases: the double flight phase, denoted by "f," in which both legs are in the air; the stance-posterior phase, denoted by "sp," in which the posterior (back) leg is on the ground; and the stance-anterior phase, denoted by "sa," in which that anterior (front) leg is on the ground.

TABLE I
Mechanical Parameters of the Model

Parameter	Value	Units
Torso Mass (m)	10.432	kg
Torso Inertia (J)	0.339	kg m^2
Hip-to-COM spacing (L)	0.138	m
Nominal Leg Length (l_0)	0.323	m
Let Spring Constant (k_{leg})	7046	N/m
Torso Spring Constant (k_{torso})	165	Nm/rad

A. Dynamics in Continuous Time

For each $i \in \{\mathrm{f}, \mathrm{sp}, \mathrm{sa}\}$, the configuration space Q_i can be parameterized by the Cartesian coordinates $(x_{\mathrm{p}}^{\mathrm{cm}}, y_{\mathrm{p}}^{\mathrm{cm}}) \in \mathbb{R}^2$ of the COM of the posterior part of the torso, its pitch angle $\theta_{\mathrm{p}} \in \mathbb{S}^1$, and the pitch angle $\theta_{\mathrm{a}} \in \mathbb{S}^1$ of the anterior part of the torso; see Fig. 2. Through the method of Lagrange, the dynamics of the model in each phase can be written in state-space form as

$$\dot{x} = f_i(x), \tag{1}$$

evolving in $TQ_i := \{x := (q', \dot{q}')' \mid q \in Q_i,\ \dot{q} \in \mathbb{R}^4\}$.

B. Event-based Transitions

Phase-to-phase transitions occur according to Fig. 3, and are triggered by leg touchdown and liftoff events modeled via suitable threshold functions, as described below.

1) Flight-to-stance Transition: The flight phase terminates when the vertical distance between the toe of either the posterior or the anterior leg and the ground becomes zero. To realize this condition, the flight state vector is augmented with the parameter array $\alpha_{\mathrm{f}} = (\varphi_{\mathrm{p}}^{\mathrm{td}}, \varphi_{\mathrm{a}}^{\mathrm{td}}) \in \mathcal{A}_{\mathrm{f}}$ containing

the angle of the posterior and the anterior leg at touchdown; see Fig. 2. It is assumed that the length of both legs at touchdown is equal to l_0, corresponding to the uncompressed length of the spring. Hence, the threshold function

$$H_{\mathrm{f}\to\mathrm{sp}}(x_{\mathrm{f}},\alpha_{\mathrm{f}}) = y_{\mathrm{p}}^{\mathrm{cm}} - L\sin\theta_{\mathrm{p}} - l_0\cos\left(\varphi_{\mathrm{p}}^{\mathrm{td}}+\theta_{\mathrm{p}}\right) \quad (2)$$

signifies the touchdown event of the posterior leg at its zero crossing. Similarly, the zeroing of

$$H_{\mathrm{f}\to\mathrm{sa}}(x_{\mathrm{f}},\alpha_{\mathrm{f}}) = y_{\mathrm{p}}^{\mathrm{cm}}+L\sin\theta_{\mathrm{p}}+2L\sin\theta_{\mathrm{a}}-l_0\cos(\varphi_{\mathrm{a}}^{\mathrm{td}}+\theta_{\mathrm{a}}) \quad (3)$$

defines the touchdown event of the anterior leg.

2) Stance-to-flight Transitions: In general, transition from stance to flight can be initiated by causing the acceleration of the stance leg end to be positive, i.e. directed upwards, when the ground force becomes zero. Due to the assumption of massless legs, the stance-to-flight condition can be simplified so that liftoff occurs when the leg obtains its natural length l_0. Consequently, the zero crossing of the threshold function

$$H_{\mathrm{sp}\to\mathrm{f}}(x_{\mathrm{sp}}) := l_0 - l_{\mathrm{p}}(x_{\mathrm{sp}}) \quad (4)$$

signifies the transition from the stance-posterior to the flight phase, while the threshold function

$$H_{\mathrm{sa}\to\mathrm{f}}(x_{\mathrm{sa}}) := l_0 - l_{\mathrm{a}}(x_{\mathrm{sa}}) \quad (5)$$

defines the anterior leg liftoff at its zeroing. In (4) and (5), l_{p} and l_{a} denote the lengths of the posterior and anterior legs as a function of the state, respectively.

C. Hybrid Dynamics of Bounding

The dynamics of the bounding gait considered here can be described by concatenating the continuous-time phases according to the sequence of Fig. 3. To study the existence of such bounding gaits, the method of Poincaré is used. The Poincaré section is taken in the extended flight phase at the apex of the spinal joint, where its vertical velocity is equal to zero; that is,

$$\mathcal{S}_{\mathrm{apex}} := \left\{ (x_{\mathrm{f}},\alpha_{\mathrm{f}}) \in \mathcal{X}_{\mathrm{f}} \mid \dot{y}_{\mathrm{p}}^{\mathrm{cm}} + L\dot{\theta}_{\mathrm{p}}\cos\theta_{\mathrm{p}} = 0, \theta_{\mathrm{a}} > 0 \right\}, \quad (6)$$

where $\mathcal{X}_{\mathrm{f}} := TQ_{\mathrm{f}} \times \mathcal{A}_{\mathrm{f}}$. As in [9], [21], to study periodic motions through fixed-point computations on a Poincaré map, the monotonically increasing horizontal coordinate $x_{\mathrm{p}}^{\mathrm{cm}}$ of the COM of the posterior part of the torso will be projected out of the state vector x_{f}. A further dimensional reduction inherent to the Poincaré method [22] can be used to substitute $\dot{y}_{\mathrm{p}}^{\mathrm{cm}}$ through the condition defining $\mathcal{S}_{\mathrm{apex}}$ in (6). Hence[1], if $\pi : \mathcal{X}_{\mathrm{f}} \to \mathcal{Z}_{\mathrm{f}}$ denotes the operator that projects x_{f} onto its non-$(x_{\mathrm{p}}^{\mathrm{cm}}, \dot{y}_{\mathrm{p}}^{\mathrm{cm}})$ components, the (reduced) Poincaré map $\mathcal{P} : \pi(\mathcal{S}_{\mathrm{apex}}) \to \pi(\mathcal{S}_{\mathrm{apex}})$ can be defined through the rule

$$z_{\mathrm{f}}[k+1] = \mathcal{P}\left(z_{\mathrm{f}}[k], \alpha_{\mathrm{f}}[k]\right), \quad (7)$$

where

$$z_{\mathrm{f}} := (y_{\mathrm{p}}^{\mathrm{cm}}, \theta_{\mathrm{p}}, \theta_{\mathrm{a}}, \dot{x}_{\mathrm{p}}^{\mathrm{cm}}, \dot{\theta}_{\mathrm{p}}, \dot{\theta}_{\mathrm{a}})', \quad (8)$$

and $\pi(\mathcal{S}_{\mathrm{apex}})$ denotes the image of $\mathcal{S}_{\mathrm{apex}}$ under π.

[1]The dimension can be further reduced due to conservation of energy.

Equation (7) represents a nonlinear discrete-time control system. The explicit appearance of the touchdown angles in the right hand side of (7) is a consequence of the dependence of the threshold functions (2) and (3) on α_{f}. It is apparent from (7) that the touchdown angles are inputs available for "cheap" control, since it is (in general) easy to place the legs during the flight phase.

III. Passively Generated Bounding Motions

This section presents a large number of passively generated fixed points corresponding to the cyclic bounding motions of interest. First, the properties of a representative bounding cycle are discussed in detail. Then, families of fixed points are computed to investigate their behavior at various energy levels, average forward speeds, and torso bending amplitudes.

A. Fixed Points and their Properties

The objective is to find an argument z_{f} in (7) that maps onto itself; this is equivalent to solving the equation

$$z_{\mathrm{f}} - \mathcal{P}\left(z_{\mathrm{f}}, \alpha_{\mathrm{f}}\right) = 0, \quad (9)$$

for physically reasonable values of touchdown angles α_{f}. The search for fixed points is conducted numerically using MATLAB's `fmincon`.

A large number of fixed points has been computed for different initial guesses and different touchdown angles. Fig. 4 and the video accompanying this paper depict the motion of the system corresponding to a representative fixed point with touchdown angles $(\varphi_{\mathrm{a}}^{\mathrm{td}}, \varphi_{\mathrm{p}}^{\mathrm{td}}) = (12.12\mathrm{deg}, 28.14\mathrm{deg})$ and initial conditions $(y_{\mathrm{p}}^{\mathrm{cm}}, \theta_{\mathrm{p}}, \theta_{\mathrm{a}}, \dot{x}_{\mathrm{p}}^{\mathrm{cm}}, \dot{y}_{\mathrm{p}}^{\mathrm{cm}}, \dot{\theta}_{\mathrm{p}}, \dot{\theta}_{\mathrm{a}})$ equal to

$$\begin{aligned}(&0.29\mathrm{m},\ -10.73\mathrm{deg},\ 10.73\mathrm{deg},\ 3.73\mathrm{m/s},\\ &0.41\mathrm{m/s},\ -172.00\mathrm{deg/s},\ -172.00\mathrm{deg/s}),\end{aligned} \quad (10)$$

respectively. Fig. 5 illustrates the evolution of the cartesian variables of the COM for both the posterior and anterior parts of the torso as well as the pitch angles and rates during one bounding cycle. The configuration variables of each leg for the bounding cycle of Fig. 5 is presented in Fig. 6. Note that Fig. 6(b) shows the absolute leg angles γ_{p} and γ_{a}, which are defined with respect to the vertical to the ground; i.e. $\gamma_i = \theta_i + \varphi_i$ for $i \in \{\mathrm{p}, \mathrm{a}\}$, see Fig. 2.

It is of interest to describe in some detail the motion of the torso during the bounding cycle corresponding to the fixed point (10). Fig. 7 presents the torso bending angle computed as the difference between the pitch angles of the anterior and posterior parts, $\theta_{\mathrm{a}} - \theta_{\mathrm{p}}$. Effectively, the anterior and posterior leg stance phases "translate" the configuration of the torso from convex to concave and vice versa in order to prepare the system for the gathered and extended flight phases, respectively. We remark that the maximum angular excursions of the torso do not appear to be tied to the touchdown events. As Fig. 7 shows, the maximum torso bending angle occurs at the middle of the extended flight phase denoted by (a), before the anterior leg touchdown. On the other hand, the minimum torso bending angle happens prior to the touchdown of the posterior leg, at the middle

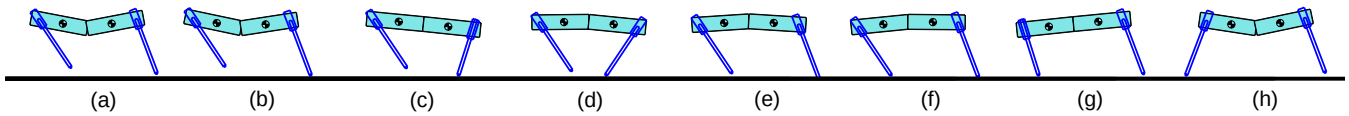

Fig. 4. Snapshots of the model during one bounding cycle. The letters refer to instants of interest as shown in Fig. 7.

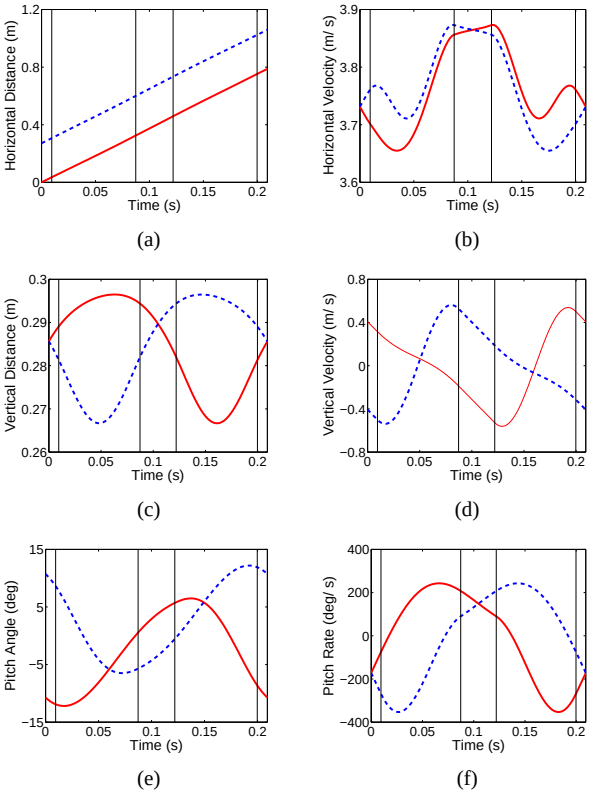

Fig. 5. Evolution of the cartesian variables and pitch angles with respect to time at a representative fixed point for the posterior (red continuous lines) and the anterior (blue dashed lines) parts of the torso. The vertical lines correspond to the events; from left to right: anterior leg touchdown, anterior leg liftoff, posterior leg touchdown, and posterior leg liftoff.

of the gathered flight phase denoted by (e). This is in agreement with observations on galloping mammals in [20], according to which maximum flexion of the spine occurs before the touchdown of the posterior leg, while maximum extension occurs prior to the touchdown of the anterior leg, contradicting Hildebrand's original findings in [17].

As a closing remark, it is worth mentioning that all the bounding fixed points computed in this work exhibit some

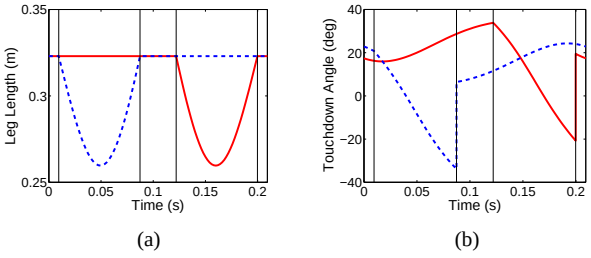

Fig. 6. Evolution of the configuration variables of the legs. (a) Leg length, l. (b) Absolute angle γ defined with respect to the vertical; see Fig. 2. The red continuous lines correspond to the posterior leg, the blue dashed lines to the anterior leg. The vertical lines signify the events as in Fig. 5.

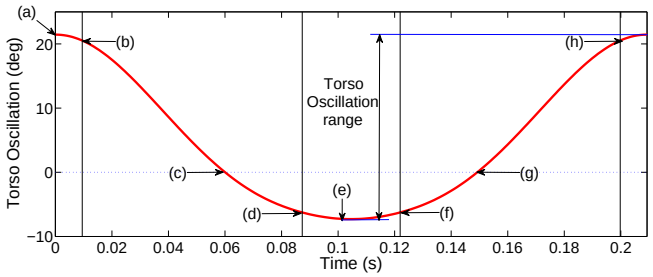

Fig. 7. Torso bending angle computed as $\theta_{\mathrm{a}} - \theta_{\mathrm{p}}$; see Fig. 2. The labels correspond to the sequence of phases in Fig. 4. From (a) to (h): apex height, anterior leg touchdown, torso flat, anterior leg liftoff, minimum torso bending, posterior leg touchdown, torso flat and posterior leg liftoff.

useful symmetry characteristics. Echoing the symmetry properties of fixed points corresponding to passively generated bounding motions on quadrupeds with rigid torso—see [9] for details—Fig. 6(b) shows that

$$\gamma_{\mathrm{a}}^{\mathrm{td}} = -\gamma_{\mathrm{p}}^{\mathrm{lo}} \text{ and } \gamma_{\mathrm{p}}^{\mathrm{td}} = -\gamma_{\mathrm{a}}^{\mathrm{lo}}. \tag{11}$$

In words, the (absolute) touchdown angle of the anterior leg is equal to the negative of the (absolute) liftoff angle of the posterior leg, and vice versa. In fact, (11) reflects a more general property of the system. Careful inspection of Fig. 5 reveals that the evolution of the states of the anterior part of the torso (blue dashed lines in Fig. 5) *forward* in time is indistinguishable from the evolution of the states of the posterior part of the torso (red continuous lines in Fig. 5) *backward* in time. Mathematically, if $G = \mathrm{diag}[1, -1, 1, -1, 1]$, then

$$x_{\mathrm{p}}(-t) = G \cdot x_{\mathrm{a}}(t), \tag{12}$$

where $x_i = (y_i^{\mathrm{cm}}, \theta_i, \dot{x}_i^{\mathrm{cm}}, \dot{y}_i^{\mathrm{cm}}, \dot{\theta}_i)'$ for $i \in \{\mathrm{p}, \mathrm{a}\}$. Equation (12) implies that G is a reversing symmetry for the vector fields of the posterior and anterior parts of the system.

B. Continuums of Symmetric Fixed Points

To further investigate the properties of passively generated bounding cycles, a large number of fixed points of the Poincaré map (7) is computed. All the fixed points presented in this section comply with the time-reversal symmetry property (12), and they all produce motions similar to the one described in detail in Section III-A. It should be mentioned here that fixed points for which the torso exhibits multiple oscillations within a single stride do exist, but have been discarded from the results presented here because these motions are not physically relevant.

Due to the conservative nature of the model, the fixed points are organized according to their total energy. The results are summarized in Fig. 8, which shows fixed points computed at three different total energy levels; namely, 180J, 200J and 220J. Fig. 8 illustrates that more pronounced torso

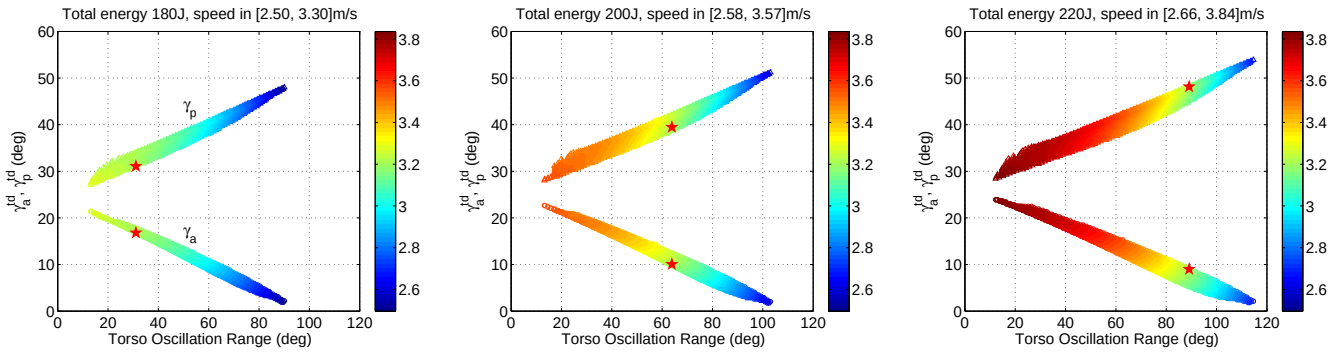

(a) (b) (c)

Fig. 8. Bounding fixed points at different total energy levels; 180J, 200J and 220J. The vertical axis corresponds to the (absolute) touchdown angles of the posterior (upper branch) and anterior legs (lower branch), γ_{p} and γ_{a}, respectively. The horizontal axis corresponds to the range of torso oscillation, see Fig. 7. The points are colored according to the average velocity computed as the ratio of the stride length over the stride period. The red stars correspond to fixed points with the same average velocity $3.2\mathrm{m/s}$ obtained at different total energies. As the total energy increases, the star "moves" to larger torso oscillation regions, which implies that maintaining the same forward speed at higher total energies results in more pronounced torso oscillations.

oscillations and higher average forward velocities can be achieved as the total energy increases. However, at a constant energy level, the torso oscillation range and the average forward speed are inversely related: larger forward speeds correspond to lower torso oscillation ranges. To provide further intuition, Fig. 9 presents the energy distribution among the modes of the motion for the fixed points in Fig. 8(b). The gravitational potential energy as well as the sum of the rotational kinetic energies of the posterior and anterior parts of the torso remain roughly constant throughout the fixed points. Given that the sum of the vertical kinetic energies of the two parts of the torso is very small, the relation between the forward motion and the torso oscillation becomes clear: fixed points at larger forward kinetic energies are associated with smaller torso elastic energies and vice versa.

It should be mentioned here that the range of forward speeds that can be realized within a constant energy level is significant—at $220\mathrm{J}$ for example, average forward velocities varying from $2.66\mathrm{m/s}$ to $3.84\mathrm{m/s}$ can be realized as Fig. 8(c) shows. This implies that a certain degree of velocity regulation can be achieved at the same total energy, and it differs from the findings in [9] for rigid torso models, in which the range of possible forward speeds within the same energy level is very narrow.

The distribution of the total energy between the forward kinetic and the torso elastic energy is determined by the touchdown angles of the system. As Fig. 8 shows, within the same energy level, a combination of smaller anterior and larger posterior touchdown angles causes more pronounced torso oscillations, resulting in lower average forward speeds. On the other hand, larger anterior and smaller posterior touchdown angles result in smaller torso oscillation, thereby increasing the speed. Clearly, the leg touchdown angles provide powerful control inputs for regulating the distribution of the total energy among these modes and thus altering the forward speed. However, direct application of intuitive controllers relating forward speed with the touchdown angles such as those in [1] is not trivial. These issues, as well as the design of controllers that take into account such properties, are currently under consideration.

C. Local Stability Properties

To investigate the local stability of the passive bounding motions computed in Section III-B, the Poincaré return map is linearized at a fixed point $(\bar{z}_{\mathrm{f}}, \bar{\alpha}_{\mathrm{f}})$ to obtain

$$\Delta z_{\mathrm{f}}[k+1] = A\Delta z_{\mathrm{f}}[k] + B\Delta\alpha_{\mathrm{f}}[k], \tag{13}$$

where $\Delta z_{\mathrm{f}} = z_{\mathrm{f}} - \bar{z}_{\mathrm{f}}$, and $\Delta\alpha_{\mathrm{f}} = \alpha_{\mathrm{f}} - \bar{\alpha}_{\mathrm{f}}$, and

$$A = \left.\frac{\partial \mathcal{P}}{\partial z_{\mathrm{f}}}\right|_{z_{\mathrm{f}}=\bar{z}_{\mathrm{f}},\alpha_{\mathrm{f}}=\bar{\alpha}_{\mathrm{f}}}, \quad B = \left.\frac{\partial \mathcal{P}}{\partial \alpha_{\mathrm{f}}}\right|_{z_{\mathrm{f}}=\bar{z}_{\mathrm{f}},\alpha_{\mathrm{f}}=\bar{\alpha}_{\mathrm{f}}}. \tag{14}$$

If all the eigenvalues of the system matrix A have magnitude less than one, then the periodic solution is stable.

Fig. 10 shows the eigenvalue with the maximum norm for the fixed points of Fig. 8. In interpreting Fig. 10 note that the data refer to the apex height of the spinal joint in the extended flight, where, in accordance to (12),

$$\theta_{\mathrm{a}} = -\theta_{\mathrm{p}} \text{ and } \dot{\theta}_{\mathrm{a}} = \dot{\theta}_{\mathrm{p}}; \tag{15}$$

Hence, two of the axes in Fig. 10 correspond to the kinetic energy associated with the torso pitch oscillation $\dot{\theta}_{\mathrm{a}} + \dot{\theta}_{\mathrm{p}} =$

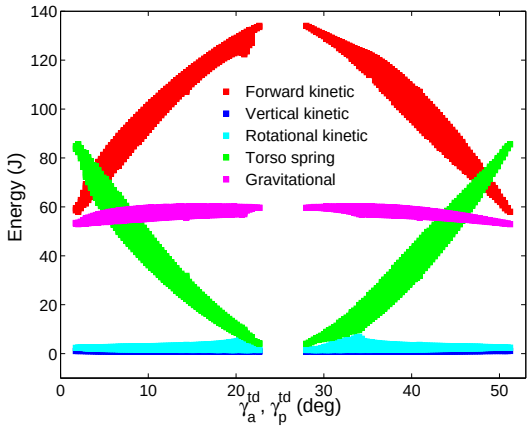

Fig. 9. Energy distribution at the apex height of the spinal joint for fixed points with total energy 200J. The horizontal axis corresponds to the (absolute) touchdown angles of the posterior (right branch) and anterior legs (left branch). The vertical axis corresponds to the energy distribution among the modes of the motion.

$2\dot{\theta}_{\rm a} = 2\dot{\theta}_{\rm p}$ and its range $\theta_{\rm a} - \theta_{\rm p} = 2\theta_{\rm a} = -2\theta_{\rm p}$. Clearly, flatter torso configurations ($\theta_{\rm a} - \theta_{\rm p} \simeq 0$) and higher pitch kinetic energies correspond to the least unstable eigenvalues. Note that this observation is reminiscent of bounding models with a rigid torso ($\theta_{\rm a} - \theta_{\rm p} = 0$), where it was found that, for given forward velocity, increasing pitch rate initially decreases the magnitude of the largest eigenvalue [9, Fig. 14]. On the other hand, pronounced torso oscillations (higher values of $\theta_{\rm a} - \theta_{\rm p}$) correspond to more unstable motions. With reference to Fig. 8, this observation implies that, for a given energy level, fixed points with smaller average forward velocities are more unstable.

While the largest eigenvalue of the majority of the fixed points of Section III-B has magnitude less than three, no fixed point that gives rise to a passively stable bounding cycle was computed in this paper. It should be mentioned here that locally stable fixed points may exist for other parameter values, and a more complete parametric analysis is the subject of ongoing work. We note briefly that the system can be nominally stabilized via a discrete LQR controller which guarantees that the eigenvalues of the linearization (13) are all within the unit disc. However, the domain of attraction of the controller is small, a fact that motivates the development of more powerful controller techniques.

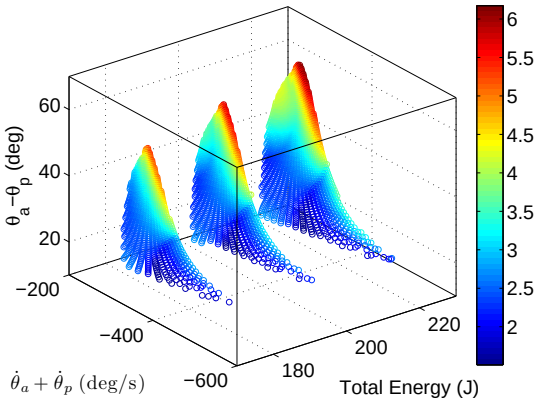

Fig. 10. Maximum eigenvalue norm of fixed points with total energy 180J, 200J and 220J. The points are located based on their energy, pitch angle and pitch rate at apex height and colored according to the maximum eigenvalue norm. None of the fixed point is passively stable.

IV. Conclusions

In this paper, the effect of torso flexibility on the generation of bounding running gaits was studied via a simple energy-preserving model. Based on the analysis of a numerically derived return map, it was found that bounding can be passively generated, as the response of the system to appropriate initial conditions. Notwithstanding its apparent simplicity, the proposed model can produce running motions in which the bending movements of the torso resemble spinal flexion and extension oscillations in galloping quadrupedal mammals. It was found that a range of forward velocities can be realized within the same total energy level depending on the touchdown angles of the posterior and anterior legs. Finally, the bounding motions computed in this work were found to be unstable.

References

[1] M. H. Raibert, *Legged Robots that Balance*. Cambridge, MA: MIT Press, 1986.

[2] I. Poulakakis, J. Smith, and M. Buehler, "Modeling and Experiments of Untethered Quadrupedal Running with a Bounding Gait: The Scout II Robot," *The International Journal of Robotics Research*, vol. 24, no. 4, pp. 239–256, 2005.

[3] M. Raibert, K. Blankespoor, G. Nelson, R. Playter, and the BigDog Team, "BigDog, the Rough-Terrain Quadruped Robot," in *Proceedings of the 17th IFAC World Congress*, Seoul, Korea, July 2008, pp. 10 822–10 825.

[4] D. Marhefka, D. Orin, J. Schmiedeler, and K. Waldron, "Intelligent Control of Quadrupedal Gallops," *IEEE/ASME Transactions on Mechatronics*, vol. 8, no. 4, pp. 446–456, 2003.

[5] J. Nichol, S. Singh, K. Waldron, L. Palmer, and D. Orin, "System Design of a Quadrupedal Galloping Machines," *The International Journal of Robotics Research*, vol. 23, no. 10-11, p. 1013, 2004.

[6] A. D. Lewis and G. A. Bekey, "Gait Adaptation in a Quadruped Robot," *Autonomous Robots*, vol. 12, pp. 301–312, 2002.

[7] R. Pfeifer, F. Iida, and J. Bongard, "New Robotics: Design Principles for Intelligent Systems," *Artificial Life*, vol. 11, pp. 99–120, 2005.

[8] N. I. Kern, R. J. Bachmann, R. J. Triolo, and R. D. Quinn, "Compliant Bodies Provide Increased Agility in Mobile Robots," in *IEEE/RSJ Conference on Intelligent Robots and Systems*, 2011, submitted.

[9] I. Poulakakis, E. Papadopoulos, and M. Buehler, "On the Stability of the Passive Dynamics of Quadrupedal Running with a Bounding Gait," *The International Journal of Robotics Research*, vol. 25, no. 7, pp. 669–687, 2006.

[10] F. Iida and R. Pfeifer, ""Cheap" Rapid Locomotion of a Quadruped Robot: Self-stabilization of Bounding Gaits," in *Intelligent Autonomous Systems 8*, F. Groen, N. Amato, E. Yoshida, and A. Bonarini, Eds. IOS Press, 2004, vol. 8, pp. 642–649.

[11] G. Zhang, Z., Y. Fukuoka, and H. Kimura, "Stable Quadrupedal Running Based Spring-Loaded Two-Segment Legged on a Models," in *Proceedings of the IEEE International Conference on Robotics and Automation*, vol. 3, New Orleans, LA, 2005, pp. 2601–2606.

[12] P. Chatzakos and E. Papadopoulos, "Self-stabilizing Quadrupedal Running by Mechanical Design," *Applied Bionics and Biomechanics*, vol. 6, no. 1, pp. 73–85, 2001.

[13] J. P. Schmiedeler and K. J. Waldron, "The Mechanics of Quadrupedal Galloping and the Future of Legged Vehicles," *The International Journal of Robotics Research*, vol. 18, pp. 1224–1234, 1999.

[14] H. Herr and T. A. McMahon, "A Galloping Horse Model," *The International Journal of Robotics Research*, vol. 20, no. 1, pp. 26–37, 2001.

[15] U. Culha and U. Saranli, "Quadrupedal Bounding with an Actuated Spinal Joint," in *Proceedings of the IEEE International Conference on Robotics and Automation*, Shanghai, China, 2010.

[16] Q. Deng, S. Wang, X. W., J. Mo, and Q. Liang, "Quasi passive bounding of a quadruped model with articulated spine," *Mechanism and Machine Theory*, vol. 52, pp. 232–242, 2012.

[17] M. Hildebrand, "Motions of the Running Cheetah and Horse," *Journal of Mammalogy*, vol. 40, no. 4, pp. 481–495, 1959.

[18] R. Alexander, N. J. Dimery, and R. F. Ker, "Elastic Structures in the Back and their Role in Galloping in some Mammals," *Journal of Zoology A*, vol. 207, pp. 467–482, 1985.

[19] R. Hackert, N. Schilling, and M. S. Fischer, "Mechanical Self-stabilization, a Working Hypothesis for the Study of the Evolution of Body Proportions in Terrestrial Mammals?" *Comptes Rendus Palevol*, vol. 5, pp. 541–549, 2006.

[20] N. Schilling and R. Hackert, "Sagittal Spine Movements of Small Therian Mammals during Asymetrical Gaits," *Journal of Experimental Biology*, vol. 209, pp. 3925–3939, 2006.

[21] R. Altendorfer, D. E. Koditschek, and P. Holmes, "Stability Analysis of Legged Locomotion Models by Symmetry-factored Return Maps," *The International Journal of Robotics Research*, vol. 23, no. 10-11, pp. 979–999, Oct. 2004.

[22] J. Guckenheimer and P. Holmes, *Nonlinear Oscillations, Dynamical Systems, and Bifurcations of Vector Fields*, ser. Applied Mathematical Sciences. New York: Springer-Verlag, 1996, vol. 42.